MODELING THE METEOROID DISTRIBUTIONS IN INTERPLANETARY SPACE AND NEAR-EARTH

Neil Divine [1,2], Eberhard Grün[2] and Peter Staubach [2]

[1] Jet Propulsion Laboratory, Pasadena, CA 91109, U.S.A.
[2] Max-Planck-Institut für Kernphysik, 69 Heidelberg, Germany

ABSTRACT

Various observational techniques have been used to study interplanetary meteoroids: groundbased zodiacal light and meteor observations, in-situ detection by spacecraft and analysis of lunar microcraters. A model of the interplanetary meteoroid environment has been developed which synthesizes all these observations. It gives numerical values for meteoroid distributions in mass, perihelion distance, eccentricity, and inclination. These distributions lead to expressions for particle flux and concentration which explicitly incorporate both Keplerian dynamics in heliocentric orbit and the directional properties of particle impact velocities for spaceborne detectors. To span the range 10^{-18} to 1 g in mass and 0.1 to 20 AU in heliocentric distance the data require five distinct populations, namely eccentric, inclined, halo, core and asteroidal (in order of increasing mean particle mass). At Earth's orbit the core and asteroidal populations dominate the meteoroid environment at masses below and above 10^{-5} g, respectively. A new technique for the evaluation of gravitational focussing by the Earth has successfully matched the meteoroid flux and angular distribution observed on LDEF surfaces near mass 10^{-6} g.

1. INTRODUCTION

Meteoroids, including interplanetary dust, are finely divided particulate matter that exists between the planets. They range in size from assemblages of a few molecules to meter-sized boulders. Sources for meteoroids are comets, asteroids, the planets and their satellites. Zodiacal light is the diffuse glow of the night sky which is caused by the reflection of sunlight from the cloud of interplanetary particles.

Different methods have been used to study interplanetary meteoroids (Fig. 1). They are distinguished by the size or mass range of particles which can be studied and by the heliocentric distance at which they have been employed. The size distribution is derived from studies of microcraters on lunar samples. Corresponding meteoroid fluxes are obtained from Earth-orbiting satellites and spaceprobes at 1 AU distance from the sun which resulted in the interplanetary flux model (Ref. 1). Orbital information is provided by radar meteor observations (Ref. 2). The radial distribution of interplanetary meteoroids ranging from 0.3 AU out to 18 AU distance from the sun was determined by the deep space probes Helios, Galileo, Ulysses, Pioneer 10 and 11. Remote observations of zodiacal light and the thermal emission of interplanetary meteoroids (Ref. 3) provide quantities integrated over all particle sizes and along various line-of-sights, however, additional parameters, like albedo and temperatures have to be assumed. Advances in refined measurements are expected from infrared observations by the COBE satellite and the inclusion of directional and speed information from the Galileo and Ulysses dust detectors will further constrain orbital distributions.

A comprehensive model describing the present state of the interplanetary meteoroid complex has been developed by Ref. 4. This model is extended to the situation near planets where gravitational focussing modifies te meteoroid fluxes. By considering the directionality of the interplanetary meteoroid flux this new model surpasses an earlier formulation of the gravitational focussing effect by Ref. 5.

2. METEOROID MODEL DESCRIPTION

2.1 Model Formulation

To obtain a quantitative description of the distributions of interplanetary meteoroids, we seek an algebraic formulation which correctly includes the particles' Keplerian dynamics in heliocentric orbit, allows the calculation of their velocities (speed and direction) relative to some detector, and specifies their concentration and flux. For each individual population (of which five will be needed to describe the entire meteoroid complex), we specify a

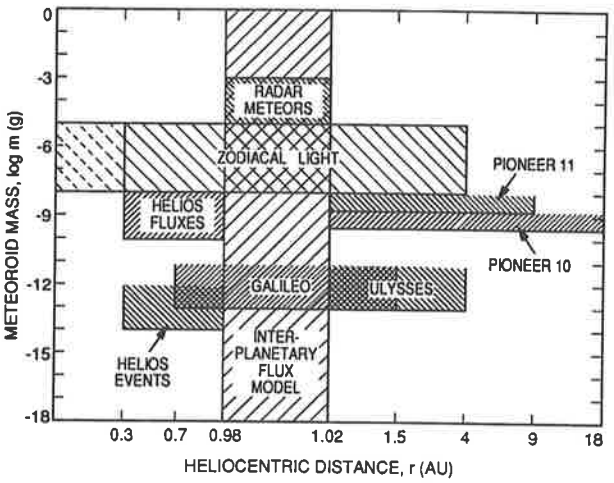

Figure 1. Coverage in mass and heliocentric distance for the data sets used in the five populations model.

distinct set of distributions in four independent variables. These four variables are the particle mass m, and the perihelion distance r_1, eccentricity e, and inclination i of the orbit. The four distributions, each of which depends on only one of these four variables, are respectively H_M (the cumulative number ratio of particles above mass m to that above $m_1 = 1.0$ gram), p_e, p_i, and N_1. The eccentricity and inclination distributions (p_e and p_i) are normalized in a way which allows the radial distribution N_1 to be interpreted as the concentration in the ecliptic plane, for mass exceeding $m_1 = 1.0$ g, and in the limit that all the eccentricities in the distribution approach zero. This formulation ensures reflection symmetry about the ecliptic plane and rotational symmetry in ecliptic longitude.

The particle density g_0 in (six-dimensional) position-velocity space, at mass m_1, can be expressed in a form which includes the product of the three orbital distributions introduced here, namely

$$g_0 = \frac{1}{2\pi e}\left(\frac{r_1}{GM}\right)^{3/2} N_1 p_e p_i \qquad (1)$$

Here the solar gravity is specified by $GM = 1.327 \cdot 10^{20}$ m^3/s^2. To obtain the concentration N_M, for mass exceeding m, at some position in interplanetary space, it is necessary to integrate Eq. 1 over all velocities, and to introduce the function H_M, with the result

$$N_M = H_M \int_{-\infty}^{+\infty} dv_x \int_{-\infty}^{+\infty} dv_y \int_{-\infty}^{+\infty} dv_z \; g_0 \qquad (2)$$

$$N_M = 4 H_M \int dr_1 \int de \int di \; \frac{\partial(v_x, v_y, v_z)}{\partial(r_1, e, i)} \left(\frac{r_1}{GM}\right)^{3/2} \frac{N_1 \, p_e \, p_i}{2 \, \pi \, e} \qquad (3)$$

In Eq. 3 a Jacobian has been introduced which transforms the differentials from the velocity components themselves to the orbital variables r_1, e, and i; in this transformation four velocity directions are possible. The limits of integration are those values for which various factors in the denominator of the Jacobian become imaginary. The result, specified in detail in Ref. 4, resembles Eq. 5.30 of Ref. 3.

Next consider a detector which has a given position, a specific heliocentric velocity $\vec{v}_{DB}$, and an efficiency η_D for the detection of particles (depending on their mass, relative impact speed, and impact direction). The flux recorded by such a detector can be expressed as an integral just like that for the concentration, except that the factor H_M is now best included in the efficiency η_D, and both that efficiency and the relative impact velocity $\mid \vec{v} - \vec{v}_{DB} \mid$ have now to appear inside the innermost of the triple integrals (Eq. 3). Evaluation of the total finally includes a sum over the four directions (l=1 to 4) within each population, and a sum over the several populations.

A thorough description of the mathematical results cited here appears in Ref. 4.

2.2 Model Development

Parameter values for the distributions comprising the several populations have been derived using a computer program whose three major activities are (1) reading data values from a file which represents all the data sets which appear in Figure 1, (2) calculating the fluxes and concentrations cited in Sec. 2.1, and (3) adjusting the distributions to best match all the data. Each data set has its own peculiarities, for example to reproduce the meteor distributions requires that weights corresponding to various observational selection effects be employed (as well as limits of integration corresponding to the bins in which the data are presented), and to reproduce the zodiacal light intensities requires integrations over particle cross-sections and along the line of sight. The separation into populations, and the adjustment of the four distributions for each population, is a task for the operator of the program, and the next paragraph provides just one example of such a process.

It has long been noticed that orbital distributions which correspond to data for radar meteors lead to concentrations which exhibit a minimum near heliocentric distance r=0.6 AU (in the ecliptic plane). This is true in particular of the meteor data used here and in Ref. 2, in which the median mass for the data set is 10^{-4} g. This becomes a useful clue to separating the populations, because the cited minimum can be considered as a cross-over between one population whose concentration increases inward and another whose concentration increases outward (on the premise that a single population should be characterized by just one maximum in each of its four distributions). Analysis of the origins of the zodiacal light suggest that the responsible population is one whose concentration increases inward, and whose dominant particle sizes are below that for the radar meteors (Ref. 3). Thus we set the mass distribution peak for the inward-increasing population small, and the other large (compared to the radar median); the two populations just distinguished form the foundations of what were later labelled the core and asteroidal populations (respectively).

Numerous other considerations, some of the same kind as that just described, led one of us (N.D.) through the development which resulted in the five populations whose detailed description appears in Ref. 4. For every data set it was required that a root-mean-square residual be minimized, between the data value and the corresponding sum of model values for the contributing populations. Samples of the distributions appear in Figures 2 and 3, whereas Figure 4 provides cumulative concentrations, in the ecliptic plane, at three mass thresholds (note the cross-over inside 1.0 AU for the core and asteroidal populations at threshold 10^{-4} g). The following paragraph summarizes the five populations, in increasing order of mean particle mass.

The eccentric population, having mean mass below 10^{-12} g, exists mostly inside 1 AU, and is based primarily on an attempt to match the angular distribution of individual impact events on Helios; it has some features in common with beta-meteoroids and is not well defined by the current data set. The inclined population, at mean mass 10^{-8} g, has particles on near-circular, moderately inclined orbits inside 1 AU; it is needed to reproduce the flux difference between the south and ecliptic sensors on Helios 1 (and has some features in common with apex particles in the literature). The halo population, at mean mass 10^{-7} g, exists beyond 2.5 AU and has random orbital inclinations (including retrograde); it is needed to provide the nearly uniform fluxes detected in the outer solar system by Ulysses, Pioneer 10, and Pioneer 11. The core population, at mean mass 10^{-5} g, has particles on orbits of small eccentricity and inclination, and increases inward (in concentration) as $r^{-1.3}$ (see Fig. 4); it bears the major responsibility for the zodiacal light, as well as making major contributions to other data sets, and is the most reliably described of the five populations. The asteroidal population, at mean mass 10^{-3} g, also has small eccentricities and inclinations, but increases outward from 1 AU; it is developed mostly from the radar meteor data, but its peak in the asteroid belt is somewhat artificial, being just large enough not to contribute too much to the zodiacal light gegenschein.

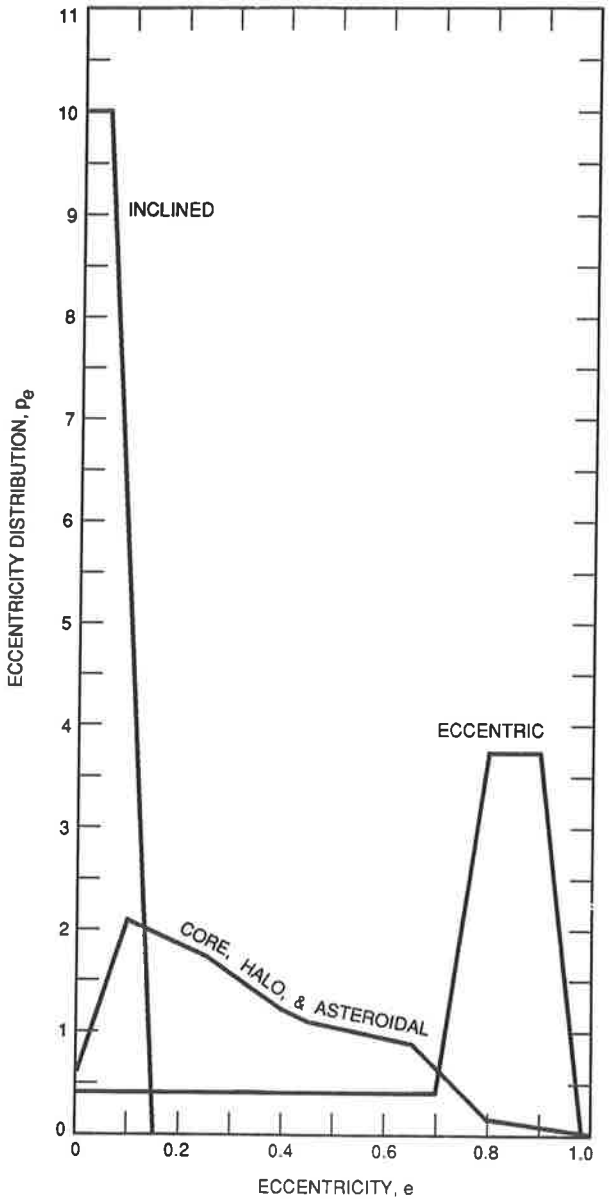

Figure 2. Eccentricity distributions for the five populations.

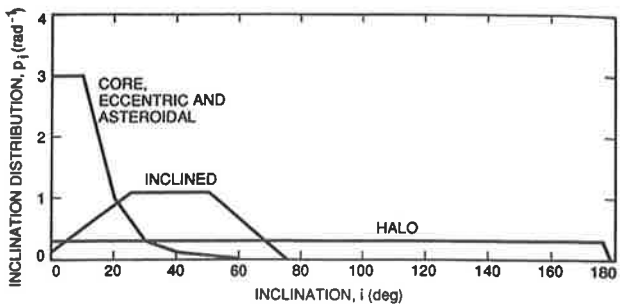

Figure 3. Inclination distributions for the five populations.

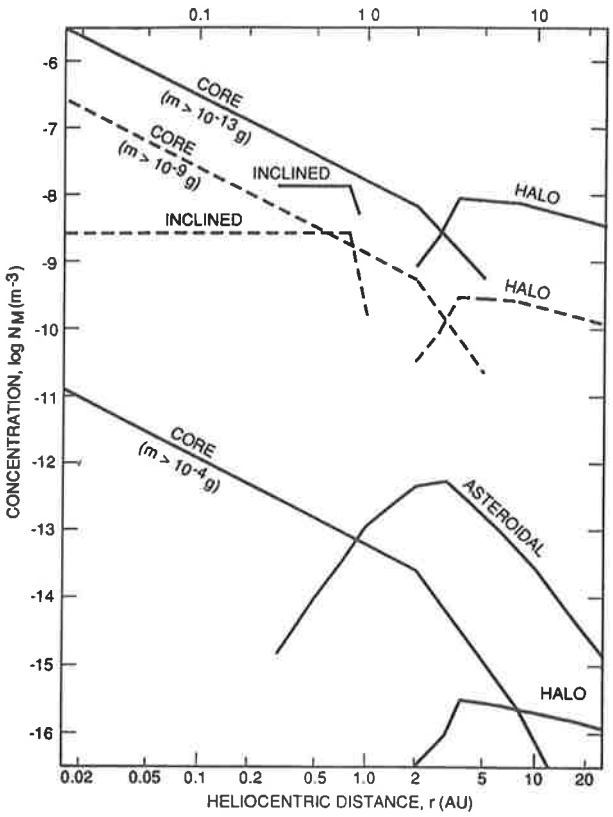

Figure 4. Cumulative number concentration as a function of heliocentric distance in the ecliptic plane for the dominant populations at three mass thresholds.

2.3 Comparison with data

The largest record of the size distribution of interplanetary dust particles has been obtained from lunar microcraters. Microcraters on lunar rocks have been found ranging from 0.02 micrometer to milimeters in diameter. Laboratory simulations of high velocity impacts on lunar-like materials have been performed in order to calibrate crater sizes with projectile sizes and impact speeds. Submicron to centimeter-sized projectiles have been used with speeds above several km/s. The crater diameter to projectile diameter has been found to vary from 2 for the smallest microcrater to about 10 for cm-sized projectiles. The difficulty to derive the impact rate from a crater count on the moon is the generally unknown exposure geometry (eg. shielding by other rocks) and exposure time of any surface on a rock. Therefore, the crater size or meteoroid mass distribution has been normalized by an impact rate measurement obtained by in-situ detectors on satellites and space probes. For submicron-sized craters significant contributions from lunar ejecta have been corrected in deriving the interplanetary flux model at 1 AU (Ref. 1).

Fig. 5 shows the contributions of the five model populations to the interplanetary flux distribution. Below 10^{-14} g the dominant population is the eccentric population. These particles have high eccentricities which are believed to be caused by the effect of radiation pressure (beta-meteoroids). The dominant contribution up to 10^{-4} g comes from the core population which is at least an order of magnitude more abundant than the halo and inclined populations. The biggest meteoroids belong to the asteroidal population.

The Galileo spacecraft was launched in 1989 and carries a dust detector through interplanetary space between Venus and Jupiter. Dust measurements were obtained between Venus' orbit and the asteroid belt, half way in between both Earth encounters (Ref. 6). The dust flux was generally larger closer to the sun than it was further away. In addition, because the sensor is facing the anti-sunward hemisphere the flux was significatly higher on the outbound leg than on the way in towards the sun. The meteoroid model - taking into account Galileo's orbit, the spacecraft atti-

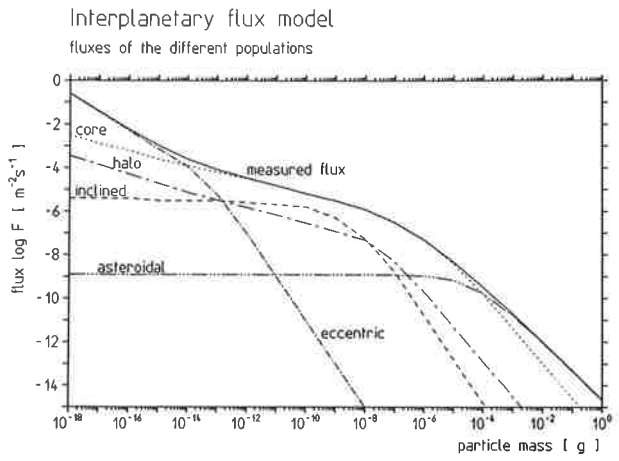

Figure 5. Contributions of the five populations to the mass distribution represented by the interplanetary flux model at r=1.0 AU in the ecliptic plane.

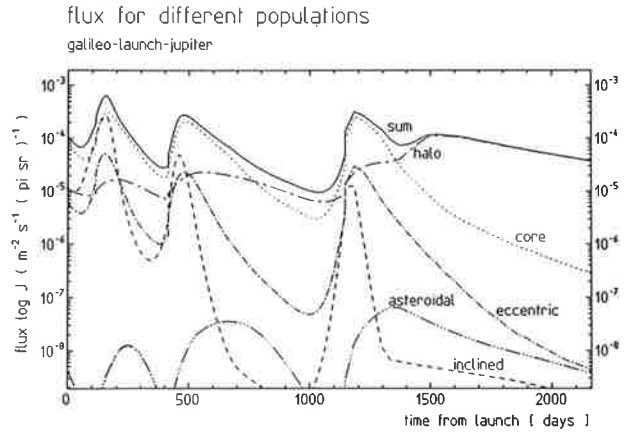

Figure 6. Contributions of the five populations to the model-poredicted flux for the Galileo dust detector. Venus and Earth fly bys took place on day 113 (V), 416 (E1), 1147 (E2) after launch, respectively.

tude, the sensor viewing and its sensitivity to different meteoroid masses - results in the flux variations shown in Fig. 6. As far as data are available the model fluxes match the observations well. Beyond about 750 days after launch the flux is a prediction which will be used to check the population parameters. For most of the time the core population dominates the flux. Only around Venus' flyby, closest to the sun, the inclined population and at distances beyond 3 AU (after 1500 days after launch) the halo population are dominant.

Table 1. summarizes the contributions of each population to each of the different data sets and hence characterizes the amount of information on a specific population which is contained in each data set. The totals (last row) suggest that the core population is accurately determined by all data sets while the eccentric population is least constrained by the measurements. Also the intermediate populations can be further refined in the future as more information becomes available.

3. FLUXES IN LOW EARTH ORBIT

3.1 Planetary Focussing

The enhancement of particle flux which results from the gravitational field of a planet has traditionally been handled using the simple result derived in Ref. 5. That result depends only on the relative magnitude of the velocity at the target point and that on approach, and not on their directions nor on the relative velocity of a particle detector. To make detailed predictions for a detector in low Earth orbit a new formulation has been developed in which the above meteoroid model and vector-velocity- dependent considerations are maintained throughout.

Here we cite only the results of the complete derivation presented in Ref. 7. For this purpose we use the symbols GM for the gravity of the planet ($GM = 3.986 \cdot 10^{14}$ m^3/s^2 for Earth), R_P for the planetary radius, and $\vec{v}_P$ for the planet's heliocentric velocity. We next consider $\vec{w}$ as the approach velocity of a meteoroid, in the absence of the planet's gravity (i.e., at infinity), as given by

$$\vec{w} = (\vec{v} - \vec{v}_P) \qquad (4)$$

DATA SET	CORE	INCLINED	ECCENTRIC	HALO	ASTEROIDAL
Interplanetary flux model	0.7	0.1	0.1		0.1
Pioneer 10	0.3			0.7	
Pioneer 11	0.4			0.6	
Helios fluxes					
ecliptic sensor	0.9	0.1			
south sensor	0.5	0.5			
Helios events					
ecliptic sensor	0.8	0.2			
south sensor	0.3	0.5	0.2		
Galileo	0.7	0.1	0.1	0.1	
Ulysses	0.3			0.7	
Radar meteors	0.4				0.6
Zodiacal light	0.7	0.1		0.1	0.1
COLUMN TOTAL	6.0	1.6	0.4	2.2	0.8

Table 1. Contributions of the five populations to the original data sets (estimated; see text of Sec. 2.3).

and $\vec{R}$ as the planetocentric position of a target point (at which we wish to evaluate the meteoroid concentration and/or flux). The particle can (possibly) reach the target point on either of two hyperbolic trajectories, and here we can specify both solutions using two auxiliary velocities, namely the radial component

$$w_R = (\vec{w} \cdot \vec{R}/R) \tag{5}$$

and the radical

$$B = +\left[\left(\frac{w - w_R}{4}\right)\left(w - w_R + \frac{4GM}{Rw}\right)\right]^{1/2} \tag{6}$$

As sketched in the plane which contains both $\vec{R}$ and $\vec{w}$, the two trajectory solutions are a clockwise one and a counterclockwise one, as distinguished by the sign which attaches to B (Eq. 6) in the relations which yield values for the vector $\vec{v}_F$, the particle's planetocentric velocity vector when it arrives at the target point. Although it is trivial to obtain the magnitude of $\vec{v}_F$, the correct calculation of its directions in the two distinct cases is more difficult.

Just as in Eq. 3 above, the evaluation of concentration and flux at the target point requires the introduction of a Jacobian, which in this case handles the transformation between the components of $\vec{v}_F$, over which the velocity integration proceeds at the target point, and those of $\vec{w}$ (i.e., in interplanetary space), whose relation to the interplanetary distributions we already know (see Sec. 2.1 above). Several pages of algebra (Ref. 7) are required to demonstrate that this Jacobian can be expressed in the form

$$\eta_F = \frac{\partial(v_x, v_y, v_z)_F}{\partial(w_x, w_y, w_z)} \tag{7}$$

$$= \left|\frac{1}{2} - \left(w - w_R + \frac{2GM}{Rw}\right)\left(\frac{\pm 1}{4B}\right)\right| \tag{8}$$

Note that whenever the approach velocity $\vec{w}$ is parallel to the target vector $\vec{R}$ we have $w_R = w$, B=0 (from Eq. 6), and an infinite Jacobian (Eq. 7), so that special care may be required to evaluate the integrals for particles which approach from close to this direction.

One further consideration is appropriate before describing how to evaluate the flux and concentration at the target point, namely for the shielding provided by the planet and its atmosphere. Omitting the messy case of deflection by the atmosphere, we consider here that this effect can be represented simply by the factor

$$\eta_s = \begin{cases} 0 & : \text{ for } \phi \text{ and } (R_P - r_1) \text{ both positive} \\ +1 & : \text{ otherwise} \end{cases} \tag{9}$$

In this expression r_1 is the periplanet distance of the hyperbolic trajectory and ϕ is the true anomaly of the particle, on that trajectory, as it reaches the target point. Note that the shielding factor η_s is zero only when r_1 is smaller than R_p and when the particle is outbound at the target (usually the two solutions are very different in the quantities r_1 and ϕ).

Both the values η_F and η_s (Eqs. 7 - 9) must be included in the innermost integrand from which the concentration or flux at the target point is to be calculated (using the triple integration discussed in Sec. 2.1). Note also, of course, that the velocity which belongs in the flux integrand is

$$\vec{v}_D = (\vec{v}_F - \vec{v}_{DP}) \tag{10}$$

where $\vec{v}_{DP}$ is the detector's planetocentric velocity at the target point (and $\vec{v}_F$ has been described above) and Eq. 10 represents the particle's velocity relative to the detector, as required in the evaluation of thresholds and efficiencies for detection (Sec. 2.1). The result for the detected flux is

$$J = \sum \int dr_1 \int de \int di \, \frac{\partial(v_x\, v_y\, v_z)}{\partial(r_1\, e\, i)} \left(\frac{r_1}{GM}\right)^{3/2} \frac{N_1 p_e p_i}{2\pi e} (\eta_F \eta_S \eta_D v_D) \tag{11}$$

Here the summation now proceeds not only over the several populations and over the four directions, but also over the two possible hyperbolic trajectories at the planet.

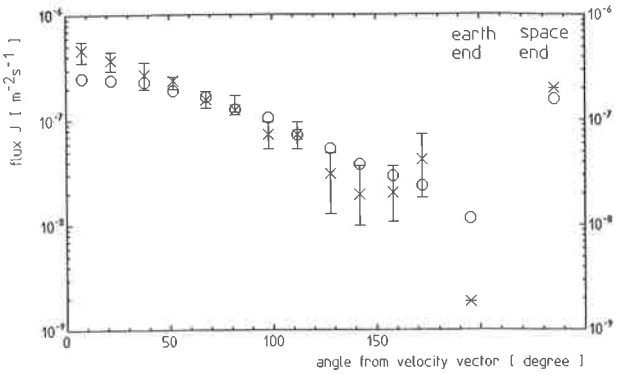

Figure 7. Comparison of model-predicted fluxes (circles) with data (crosses) from Ref. 8. These results for LDEF, as functions of angle from the velocity vector, include the effects of both gravitational focussing and atmospheric shielding on the distributions for the meteoroid model in the absence of the Earth.

3.2 Results for LDEF

The Long Duration Exposure Facility LDEF was orbiting the earth for 69 months. Among other experiments meteoroids and space debris impacts were detected on its fourteen faces. LDEF was a three-axis gravity-gradient stabilized spacecraft, so one end was always pointed towards the center of the earth while the other end was pointed into deep space. One side was always faced in the travel direction (Row 9), one in the opposite direction and two of its 14 faces were parallel to the velocity vector. The three angles which characterized the orientation of the spacecraft are named pitch, yaw and roll. Unfortunately a misalignment caused about 8 degrees in yaw and 1 degree in pitch so that the leading edge was between row 9 and row 10 and the space-facing end of LDEF was pointed slightly (1 degree) to the forward direction of flight.

Fig.7 shows the results of the crater flux around the LDEF published by Humes (Ref. 8), for a threshold crater diameter of 0.5 mm. Various approaches were made to model the absolute flux values as well as the angular dependence to the velocity vector. Good agreement with the measured values was obtained using only the core poplation to match the data because this population is dominant in the considered mass range near 10^{-6} g, a threshold which corresponds approximately to that in crater size. It was necessary for the computer program to average over the LDEF orbiting time (about 90 minutes), to average over the LDEF precession of node and to average over the earth orbit around the sun. All the correct velocity relations with respect to the orientated surfaces have to be maintained. Also the offsets in pitch and yaw which have influence to the velocity relations had to be taken into consideration. Fig.7 shows the agreement between the model and the measured values. Only for the leading edge and for the earth and the space end of LDEF there is a little discrepancy between the model predicted values and the measured data.

4. REFERENCES

1. Grün, E., H.A. Zook, H. Fechtig and R. H. Giese, Collisional Ballance of the Meteoritic Complex, *Icarus*, 62, 244-272, 1985

2. Sekanina, Z., and R. B. Southworth, Physical and Dynamical Studies of Meteors: Meteor Fragmentation and Stream-Distribution Studies, *NASA CR-2615*, 94 pp., 1975.

3. Leinert, C. and E. Grün, Interplanetary Dust, in Physics of the Inner Heliosphere I, edited by R. Schwenn and E. Marsch, *Springer-Verlag,Berlin*, p. 207-275, 1990

4. Divine, N., Five Populations of Interplanetary Meteoroids, *JGR-Planets*, 1993, in press

5. Öpik,E. J., Collision Probabilities with the Planets and the Distribution of Interplanetary Matter, *Proc. Royal Irish Academy*, 54A, 165-199, 1951.

6. Grün, E., M. Baguhl, H. Fechtig, M. S. Hanner, J. Kissel, B.-A. Lindblad, D. Linkert, G. Linkert, I. Mann, J.A.M. McDonnell, G.E. Morfill , C. Polanskey, R. Riemann, G. Schwehm, N. Siddique and H.A. Zook, Galileo and Ulysses Dust Measurements: From Venus to Jupiter, *Geophys. Res.Lett.*, 19, 1311-1314, 1992

7. Divine, N., Meteoroid Focussing at a Planet, *JPL Interoffice Memorandum* 5217-92-86, 1992.

8. Humes, D. H., Large Craters on the Meteoroid and Space Debris Experiment, *First LDEF Post-Retrieval Symposium, NASA CP-3134*, p. 399, 1991.